https://www.scirp.org/journal/jbise
J. Biomedical Science and Engineering,
2025, Vol. 18, (No. 4), pp: 113-137

A Semi-Automatic Leukocyte Tracking (SALT) Method for *in Vivo* Leukocyte Rolling and Adhesion Analysis

Spencer Thomas*, Hugo Montejo*, Ashlee Baker, Sheron Sheravina Puti, Jianjie Wang*#

Department of Biomedical Science, Missouri State University, Springfield, U.S.A

Correspondence to: Jianjie Wang, Jwang@missouristate.edu
Keywords: Leukocyte Rolling, Adhesion, Leukocyte Tracking, ImageJ/Fiji, *In Vivo*
Received: October 25, 2024 **Accepted:** April 25, 2025 **Published:** April 28, 2025

ABSTRACT

The study aims to develop a semi-automatic leukocyte tracking (SALT) method to efficiently quantify *in vivo* leukocyte rolling and adhesion, overcoming the time-consuming limitations of manual frame-by-frame analysis of time-lapse images. This computational approach enables the rapid processing of large data sets, facilitating the study of leukocyte rolling and adhesion, initial and important events for leukocyte recruitment during tissue inflammation. Leukocytes were detected and tracked using the customized SALT module in ImageJ/Fiji, following specified criteria. Leukocyte flux, rolling, and adhesion were quantified from the tracks using a conditional decision algorithm. To validate the SALT method, the same images were analyzed in parallel by independent analyzers using both the SALT method and the classical manual tracking technique for comparison. The novel SALT method demonstrated high inter-rater and intra-rater reliability for rolling velocity, with no significant differences observed. Strong correlations were found between SALT and manual measurements for leukocyte displacement and velocity ($r = 0.96$, $r = 0.97$; $p < 0.001$), total and rolling flux ($r = 0.81$, $r = 0.89$; $p < 0.05$), and adherent cells ($r = 0.97$, $p < 0.001$). The SALT technique will be implemented to eliminate subjective bias and enhance high-throughput *in vivo* leukocyte rolling and adhesion analysis using ImageJ/Fiji in future studies.

1. INTRODUCTION

Inflammation plays a pivotal role in human health and disease, encompassing processes from pathogenesis to tissue repair [1-3]. Circulating leukocytes are central to the inflammation responses, migrating to sites of injury or infection where they initiate and regulate immune responses. These cells recognize and

*Co-first authors.
#Corresponding author.

eliminate pathogens, clear damaged cells, and release signaling molecules essential for resolving inflammation and promoting tissue repair. However, inflammation is a double-edged sword; while it is vital for defense and healing, excessive or dysregulated inflammatory responses can damage normal tissues, contributing to various diseases and disorders.

In addition to the role of resident tissue immune cells, the cardiovascular (hemodynamic) response is equally critical in inflammation4. Localized mechanical stimulation or insults—such as ischemia, nutrient deprivation, or immune activation—trigger an immediate response characterized by blood vessel dilation, vascular leakage, and leukocyte infiltration. Within post-capillary venules, activated leukocytes and endothelial cells upregulate adhesion molecules and pro-inflammatory mediators, facilitating leukocyte rolling, adhesion, and eventual extravasation to the site of injury.

It is worth noting that leukocyte extravasation also occurs under normal conditions to maintain tissue homeostasis and respond to minor injuries or infections [4]. This process is tightly regulated, with minimal leukocyte-endothelial interaction maintained by the inhibitory effect of high wall shear stress generated by fast blood flow velocity [5-7]. Therefore, understanding of the mechanisms underlying inflammatory responses is critical for developing effective therapeutic strategies.

Two principal methods for studying leukocyte-endothelial interactions include endothelial monolayer flow chambers and intravital microscopy. *In vitro* techniques such as leukocyte trans-endothelial migration and parallel-plate flow chamber assays have provided critical insights into microvascular roles in vascular permeability and immune cell homing during inflammation. Additionally, advances in computerized and digital cell tracking technologies have improved the precision and efficiency of *in vitro* analyses. However, *in vitro* approaches are inherently limited, as experimental conditions often fail to fully replicate the complexity of mechanisms occurring in the body. Consequently, *in vivo* studies remain indispensable for advancing our understanding of leukocyte behavior and its broader physiological implications [6, 8, 9].

Intravital microscopy provides invaluable real-time observations of leukocyte behavior in the circulating vasculature; however, *in vivo* studies face significant challenges due to the intricate and dynamic nature of the microvascular environment. This study focuses on addressing the critical challenges of *in vivo* image analysis. Two primary issues include: (1) the labor-intensive nature of traditional manual frame-by-frame analysis, and (2) the failure of existing automated tracking systems, which are primarily developed for *in vitro* analysis using centroid- and correlation-based trackers [10-14], to perform effectively on *in vivo* images. The unique complexities of *in vivo* imaging—such as high background noise, cellular heterogeneity, motion blur, and the constantly changing microvascular structure—exacerbate these challenges, rendering current automated tracking systems inadequate [10, 15, 24-26, 16-23].

To address these challenges, the current study aimed to design and implement a novel semi-automated leukocyte tracking (SALT) method. This method integrates advanced image analysis tools and principles of hemodynamics to enable more accurate and efficient tracking of leukocyte movement *in vivo*. By leveraging neural-network-based decision frameworks, SALT overcomes the limitations of conventional centroid and correlation-based trackers, offering a robust solution for analyzing leukocyte-endothelial interactions in complex biological environments.

2. MATERIALS & METHODS

2.1. Experimental Animals & Cremaster Muscle Preparation

All animal care and research were conducted in compliance with the Guide for the Care and Use of Laboratory Animals of the National Research Council under protocols that were approved by the Institutional Animal Care and Use Committee of the Missouri State University.

Studies were carried out on male C57BL/6 mice. The mice were purchased from the Jackson Laboratory and then bred in the animal facility at Missouri State University. Male mice with 8 - 12 weeks old and 21 - 30 g body weight were used for the study. Mice were anesthetized via an intrapleural injection of 150 mg/kg ketamine and 11.25 mg/kg xylazine (Med-Vet International) in a mixed solution.

The cremaster muscle preparation was modified from a previous method [27]. Briefly, the animal was

placed supine on a custom Plexiglass tray with a water circulator (Fisher Scientific™, Model 9005) to maintain a body temperature of 37˚C. After fur removal and skin disinfection, an incision was made from the scrotal apex to the inguinal fold, and the sac was carefully opened. The epididymis, testes, and spermatic cord were separated from connective tissue and repositioned into the abdomen via the inguinal canal. The main vasculature of the cremaster muscle was centered on a quartz pillar.

During tissue preparation, the muscle was continuously superfused with Krebs solution at 37 ± 1˚C, followed by a 30-minute equilibration on the microscope stage. To label leukocytes, Rhodamine 6G (0.67 mg/kg, Fisher Scientific™) was administered intravenously via the lateral tail vein.

Venules were identified by their converging blood flow pattern, in contrast to the divergent flow pattern in arterioles. The venule selection criteria were based on standards from Ley K, [13, 14, 28, 29], Granger DN, [6, 7, 30] and Gavins [31]. Briefly, a selected venule had to be unbranched within the region of interest (ROI), 20 - 40 μm in diameter, >100 μm in length, maintain intact blood flow during recording, and exhibit high-velocity, free-flowing leukocytes.

2.2. Image Acquisition

Images were captured by a side-mounted CCD EXi Blue camera (QImaging, British Columbia, Canada) attached to an IX81 Olympus microscope, operated by Micro-manager [32] (open source; https://micro-manager.org/). A 10X objective lens (UPlanFL N 10x, NA 0.3, WD 10MM, Fluorite UP-LFLN10X2) and a Semrock Brightline CY3 filter set (Ex531/40, 562DM, Em593/40) were used for Rhodamine 6G to detect leukocytes, illuminated by a Xenon Burner (UXL-75XB 75W Short Gap). Time-lapse images were captured at 14 bit; 30 Mhz.

The centerline blood velocity was assessed by measuring the centerline velocity of red blood cells (V_{rbc}) in the lumen center of the venule, using bright-field imaging captured at 30 - 40 fps for 100 - 120 frames. Fluorescent time-lapse images were captured at consecutive time point intervals (0 min, 5 min, 10 min, 15 min, 30 min, 45 min, 60 min) for each indexed venule for 60 sec at 12.5 fps (**Figure 1**).

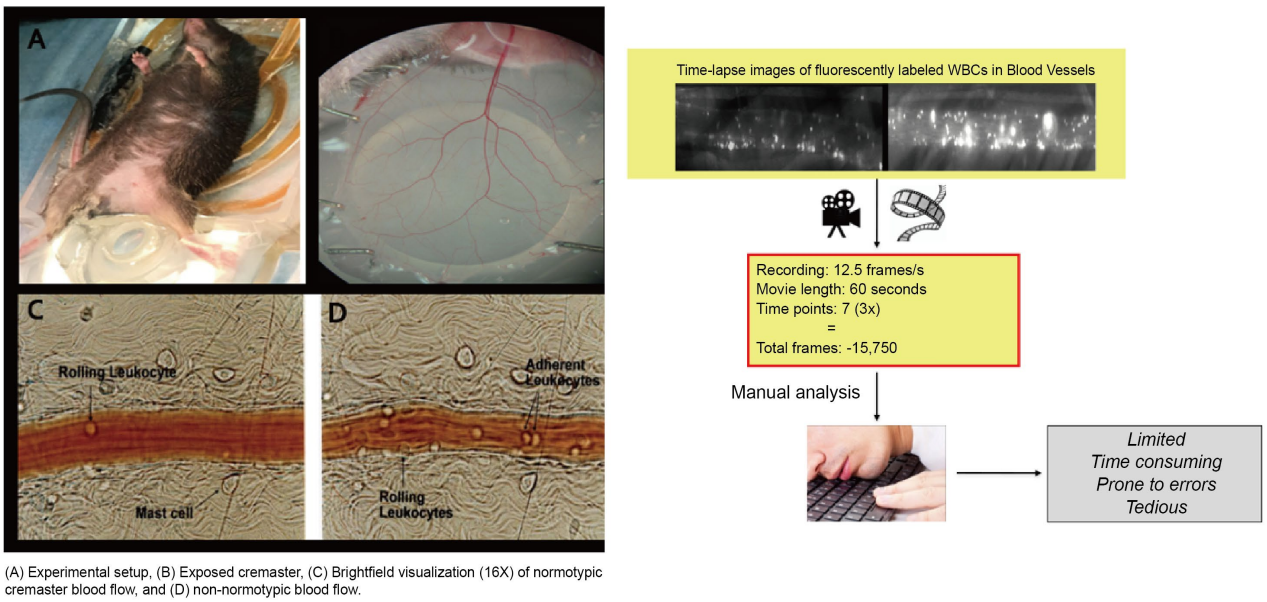

Figure 1. Representative bright-field (BF) and fluorescent images. Left panel: (A) A male mouse positioned on a tray with a water circulator to maintain body temperature of 37˚C. (B) The cremaster muscle laid on a quartz pillar. (C, D) BF images captured using intravital microscopy. Right panel: Representative fluorescent images showing neutrophils labeled with Rhodamine 6G.

2.3. Image Pre-Processing: Background Registration and Stabilization

Off-line image analysis was conducted using ImageJ 1.51. Time-lapse images (100 frames) were acquired at 30 - 45 fps. To determine venule diameter, we converted pixels to distance by applying a correction factor of 1.54 pixels/μm, which was obtained through measurement with an Objective Micrometer (Olympus). Given that motion artifacts from tissue movement, respiration, and hemodynamic flow can significantly distort image data, we implemented a rigorous image registration and stabilization protocol based on the method described by Goobic [33]. Briefly, stable background regions, identified as areas free of motion artifacts and consistent across frames, were selected. These stable regions were then used to construct a background template, which served as a reference for aligning subsequent frames. This template correction minimized background fluctuations, intensity variation, and motion distortions. The full methodology is outlined in **Abbreviations**.

After background registration, an imageJ macro, Stack CLAHE (Contrast Limited Adaptive Histogram Equalization) (https://imagej.net/Enhance_Local_Contrast_(CLAHE)) was used to ensure consistent pixel intensity scaling across the image stack by enhancing local contrast. For precise alignment, the ImageJ StackReg plugin, using a normalized cross-correlation algorithm for sub-pixel registration, was applied with a maximum displacement threshold of 10 pixels.

After stabilization, microvascular structures were enhanced using the unsharp mask filter with a radius of 1.5 pixels and a mask weight of 0.6 to improve edge definition for vessel segmentation. This enhancement step was critical for optimizing vessel segmentation.

Following template matching and stabilization, a background subtraction macro (see **Abbreviations**) was used to normalize each image frame to a background ROI (5 × 5 pixels) selected by the user to represent an area corresponding the image intensity minima. Additional compensatory steps, adapted from Goobic *et al.* (2005) [33], were implemented to address background motion artifacts (see **Abbreviations**).

2.4. Image Enhancement and Processing

To improve signal-noise ratio (SNR) and eliminate image artifacts, image enhancement and processing were conducted (**Table 1**). Key artifacts included background noise, stochastic noise, motion artifacts [34]. First, images were enhanced using an edge detection and morphological intensity filter. The macro applied a local contrast enhancement filter ("blocksize = 2, histogram = 256, maximum = 2, mask = *inverted*"), followed by a median intensity filter (0.5-pixel diameter) and Gaussian blur (0.5-pixel diameter) to refine image quality [35]. Image segmentation was then performed to selectively enhance the leukocyte pixels.

Table 1. Summarized techniques used in image pre-processing, enhancement, and processing.

Category	Image Technique	Description	Image Type Performed On[a]
Pre-processing	Pixel-brightness transformations	Adjusting intensity values to normalize brightness across frames based on image intensity histogram (0 - 255).	BF, F
	Background detection and image registration[b]	Stabilizing images to correct for motion artifacts using the Goobic *et al.* method [33].	BF, F
	Vrbc 5.1 macro	Pre-processing filter for Optic flow analysis[d].	BF
Image Enhancement	Local contrast enhancement filter	Contrast Limited Adaptive Histogram Equalization (CLAHE) applied for improved vessel and cell contrast [36].	BF, F

Continued

	Background Subtraction macro	Remove background based on image intensity minima, minimizing false positives[d].	F
	Unsharp masking	Enhancing edge definition of vascular structures to improve segmentation accuracy.	BF, F
Segmentation & Detection	Image thresholding, binarization, and segmentation	Thresholding based on Renyi entropy to isolate leukocytes from background noise [37].	F
	Leukocyte detection via morphological LoG intensity filters	Identification of leukocytes through TrackMate-based particle tracking using Lapacian of Gaussian filter (LoG) [38].	F
Tracking & Analysis	Particle Image Velocimetry (PIV)	Generating velocity vector fields to assess blood flow and leukocyte movement [39].	BF
	Optical flow analysis (FlowJ)	Estimating leukocyte movement by tracking pixel intensity changes between frames) [20].	BF
	V_{rbc} estimation	Estimation of centerline red blood cell velocity using optic flow computation [40].	BF
	LAP[c] based Kalman f iltering for leukocyte track prediction	Motion prediction and noise reduction in leukocyte tracking using predictive modeling.	F

[a]BF (bright field) or F (fluorescence) images, [b]Each image was matched to a template image, removing intensity and motion artifacts (background noise, motion artifacts), [c]LAP (linear assignment problem). [d]See **Abbreviations** for additional information.

2.5. Optical Flow-Based Blood Flow Analysis

Optical flow, a method that tracks the movement of pixels between consecutive frames in an image stack, was used to assess blood flow in a vessel. This computational imaging technique estimates the apparent motion of intensity patterns between consecutive frames, making it widely applicable in blood cell tracking and fluid motion studies. Optical flow assumes that the intensity (brightness) of a moving pixel remains constant between consecutive frames, the motion of pixels is small enough to be approximated linearly, and that neighboring pixels typically exhibit similar motion. Mathematically, optical flow is represented as,

$$I_x V_x + I_y V_y + I_t = 0 \tag{1}$$

In this equation, I_x and I_y represent the spatial intensity gradients (changes in brightness along the x and y axes), I_t is the temporal intensity gradient (intensity change over time), and V_x and V_y are the velocity components of motion in the x and y directions. Since this equation contains two unknowns (V_x and V_y), additional constraints are needed for a unique solution. There are typically provided by methods such as the Lucas-Kanade method, which estimates motion locally using small pixel windows, or the Horn-Schunck method, which enforces a global smoothness constraint across the image.

Optical flow was performed in ImageJ using the Particle Image Velocimetry (PIV) plugin (https://sites.google.com/site/qingzongtseng/piv) to create velocity vector fields with the ImageJ FlowJ plugin to ultimately compute the optical flow analysis and derive the V_{rbc}.

2.5.1. Particle Image Velocimetry (PIV)

Following brightfield image registration, linear flow "streak" profiles were created using the PIV plugin to produce velocity and direction vectors profiles. The PIV method implements a cross-correlation algorithm based on the Horn-Schnuck method and is applied globally. To ensure accurate flow modeling, vessel centerlines were extracted and the local flow vector at any given pixel (x, y) was computed by identifying the 10 nearest centerline pixels, denoted as NCLP (x, y) (see **Abbreviations**). The directional angle of the centerline segment was determined by averaging the angles between adjacent pixels, providing a smooth estimate of local flow direction.

Since vessel topology alone cannot distinguish between opposing flow directions, an initialization step was required. This involved tracking flowing RBCs over five consecutive frames and calculating their median motion direction. The final virtual flow direction VF (x, y) was assigned the angle closest to the median motion vector, resolving ambiguities within $\pm\pi/2$.

2.5.2. Optical Flow Computation of V_{rbc} Using FlowJ

Following PIV analysis, the V_{rbc} 5.1 macro (see **Abbreviations**) was ran on the images produced, and the optic flow velocity profiles were then used to derive the centerline velocity at a given point, computed for each frame pair (T_2- T_1) and analyzed in FlowJ utilizing the Lucas-Kanade algorithm using parameters σ_s = 0.5, σ_t = 1.0, σ_w = 1.0, τ = 1.0. The resulting horizontal (V_x) and vertical (V_y) displacements were used to determine instantaneous velocity ($\vec{V}_{xy}$).

$$\vec{V}_{xy} = \sqrt{\left(V_x\right)^2 + \left(V_y\right)^2} \tag{2}$$

These vectors were then used to estimate the V_{rbc}, in pixels per frame **(Figure 2)**. The velocity profiles were cross-checked against known velocities, conducted by manual V_{rbc} estimation, and that of the velocity profiles yielded by the PIV plugin. Subsequently, the instantaneous velocity magnitude between two frames computed from FlowJ was measured over 3 - 5 sequential frames in a fixed region, in triplicate. If no deviation was observed for the three independent measures, the optical flow was computed for the entire experimental time frame (100 frames), yielding the mean centerline red blood cell velocity (V_{rbc}).

2.6. Assessing V_{avg} and V_{crit}

Once the V_{rbc} for an image was obtained from optical flow, the average blood flow velocity (V_{avg}) was determined by dividing V_{rbc} by an empirical factor of 1.6 using Equation (3) and the venular wall shear rate (γ_w) [41-43] was computed using Equation (4)

$$V_{avg} = V_{rbc}/1.6 \tag{3}$$

$$\gamma_w = 2.12 \cdot 8 \cdot V_{avg}/D_v \tag{4}$$

where V_{avg} represents the average blood flow velocity and the white blood cell velocity, V_{wbc}, approximates V_{avg} [7, 13, 44] and D_v was the venular diameter previously measured using the image caliper as described in the Methods section 2.3. The critical velocity (V_{crit}) was defined as the lowest or threshold velocity at which leukocytes are assumed to minimally interact with the vascular wall, calculated as

$$V_{crit} = V_{avg} \cdot \varepsilon\left(2 - \varepsilon\right) \tag{5}$$

where ε was the ratio of leukocyte diameter to the venular diameter. In addition, all hemodynamic parameter symbols are listed in (**Table 2**).

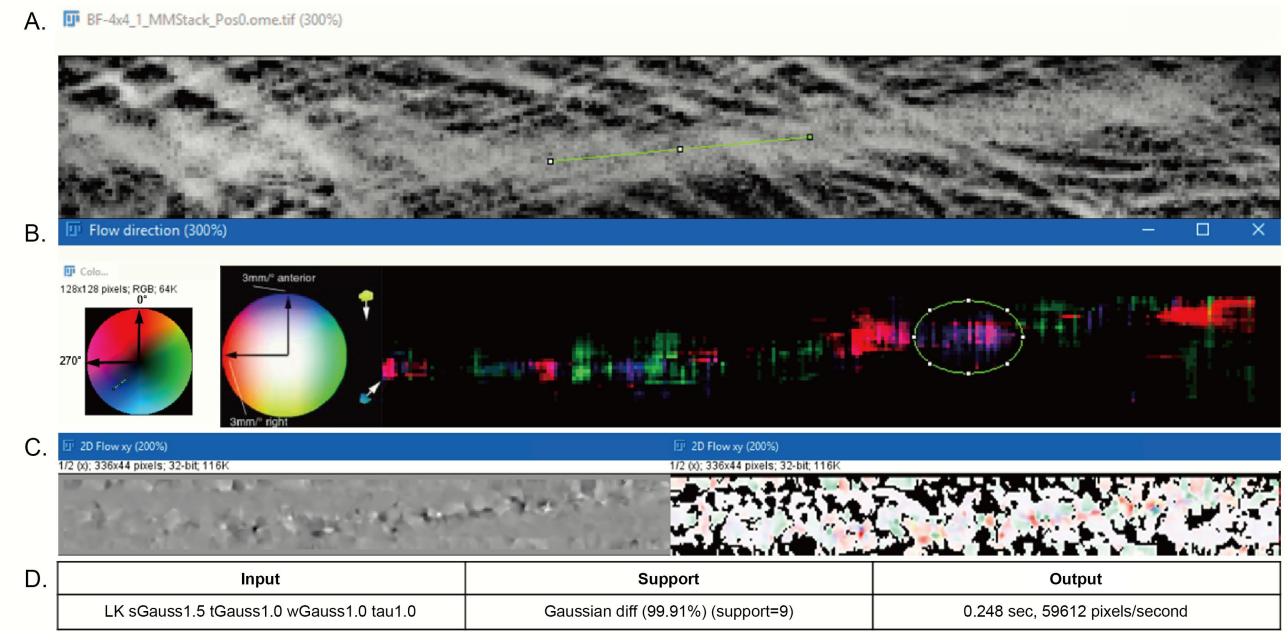

Figure 2. Optic flow estimation fields. (A) Representative images of optic flow vector fields for the original inverted 8-bit image. (B) Flow direction field with corresponding color-coded orientation and magnitude field. (C) Filtered and segmented *xy* velocity vector field. (D) Estimated quantification of vector displacement field. Selection for the correct orientation of flow was the area defined by user and significant points were determined by FlowJ support variable (Gaussian diff > 99.00%). The output computation time and V_{xy}, were then converted into V_{rbc} using previous time and pixel-μm calibrations.

Table 2. Hemodynamic parameters for leukocyte rolling by intravital microscopy.

Parameter	Symbol	Equation	Definition	Unit
Vessel diameter	D_V	Exp.	Maximal orthogonal distance between endothelial cells on opposite sides of vessel (inner diameter)	μm
Leukocyte diameter	D_L	Constant	Normal diameter of free-flowing leukocyte; ~7 μm	μm
Diameter ratio	ε	D_L/D_v	Cell to vessel diameter ratio [45]	
Centerline velocity	V_{rbc}	Exp.	Centerline velocity of RBCs; converted into average using empirical correction factor [46]	μm/s
Mean blood flow velocity	V_{avg}	$V_{rbc}/1.6$	Typically ~60% of the commonly measured centerline velocity [40]	μm/s
Critical velocity	V_{crit}	$V_{avg}\cdot\varepsilon(2-\varepsilon)$	Minimal V_{avg} of free-flowing leukocytes close to vessel wall without contact or interaction with endothelial	μm/s
Wall shear rate	γ_W	$8\cdot V_{avg}/D_v$	Frictional force at vessel wall preventing leukocyte adhesion	s^{-1}
Total leukocyte flux	TF	Exp.	Number of leukocytes that pass through a vessel per minute for a given experiment	n/min

Continued

Rolling flux	RF	Exp.	Number of rolling leukocytes ($V_{avg} < V_{CRIT}$) in a defined segment of a vessel per minute	n/min
Adherent cells	A	Exp.	Number of adherent leukocytes per mm^2 for a given observation period	n/100 μm
Mean squared displacement	MSD	$\frac{1}{N-n}\sum_{i=1}^{N-n} d^2$	Measure of the deviation of the position of a particle with respect to a reference position over time	μm^2

Experimental (Exp.).

2.7. Fluorescence Image Segmentation

Image segmentation was performed on 8-bit or 16-bit images using intensity thresholding, binarizing them into two intensity values (0 or 1). Following image pre-processing and optical flow analysis, image segmentation in ImageJ improved cell tracking efficiency by reducing computational runtime and false positives [47]. The auto-threshold plugin applied global thresholding methods, including Huang, Intermodes, Otsu, IsoData, MaxEntropy, Percentile, and RenyiEntropy based on histogram intensity.

RenyiEntropy threshold filter was selected [37, 48] due to its effectiveness in high-entropy image sequences. It has been shown to differentiate leukocyte nuclei in peripheral blood smears and selectively isolates fluorescent leukocytes [37]. Studies, including Ghosh *et al.* (2011) have demonstrated its efficacy in segmenting leukocytes in images of intravital microscopy. Additionally, RenyiEntropy thresholding has been shown to efficiently separate leukocytes from the background in microvascular environments, even under low-contrast conditions. It outperformed standard methods, such as Otsu's, particularly in images with non-uniform lighting or when leukocytes were partially obscured by other cells or tissue structures [48].

Additionally, RenyiEntropy thresholding effectively handles noisy images. Wu *et al.* (2019) found it more robust than traditional methods, providing accurate segmentation in IVM images. This robustness is crucial for tracking leukocyte behavior *in vivo*, where subtle intensity differences might otherwise be misclassified [49].

To enhance thresholding accuracy, users first defined a manual ROI representing each frame's intensity maxima and minima, then applied the auto-contrast feature in ImageJ to adjust thresholding based on the image's intensity histogram. Once an ROI including a representative cell, vessel wall, and background was selected, the RenyiEntropy algorithm analyzed the histogram, calculated total entropy for all possible thresholds, and determined an optimal threshold.

The algorithm generated an output video with threshold values, where pixel intensities >120 were classified as foreground and ≤120 as background. Running the algorithm independently on each frame—an adjustable parameter—ensured optimal threshold selection for diverse images. The segmentation process converted grayscale pixels (0 - 255) into binary (0 or 1), simplifying data for computer vision analysis [50]. Pixels below the threshold were set to black ("0"), while those above were set to white ("1"), facilitating accurate cell detection and tracking using the SALT module (**Figure 3**).

2.8. Leukocyte Detection and Spatiotemporal Tracking

Following fluorescence image enhancement and binarization, leukocyte detection was performed using ImageJ's TrackMate plugin with the Laplacian-of-Gaussian (LoG) filter, further described in previous studies [19, 51-53]. Parameters for LoG-based spot detection were customized for intravital conditions: a spot diameter of 10 μm and intensity threshold of 5 ± 2.5, based on the filtered image's local maxima. These settings accounted for contrast and resolution changes introduced during pre-processing (**Figure 4**).

After leukocyte indexing, we introduced a semi-automated framework to track cell trajectories across

sequential frames. A modified Linear Assignment Problem (LAP) tracker was implemented in TrackMate, utilizing a Kalman filter for predictive modeling.

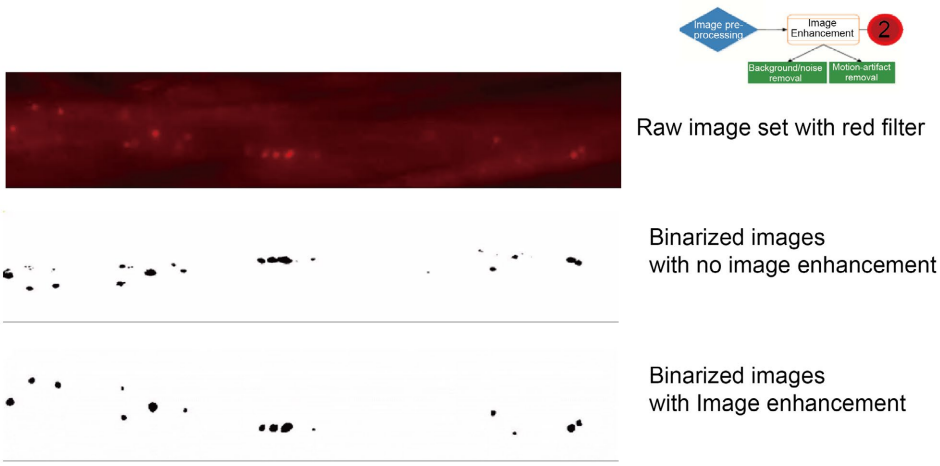

Figure 3. Representative enhanced and binarized leukocyte images using *RenyiEntropy* threshold filter. Leukocytes in cremaster venule were labeled with R6G. Top: Pseudo-red color filter applied. Middle: Unenhanced image and its binarized version. Bottom: Enhanced image with binarization.

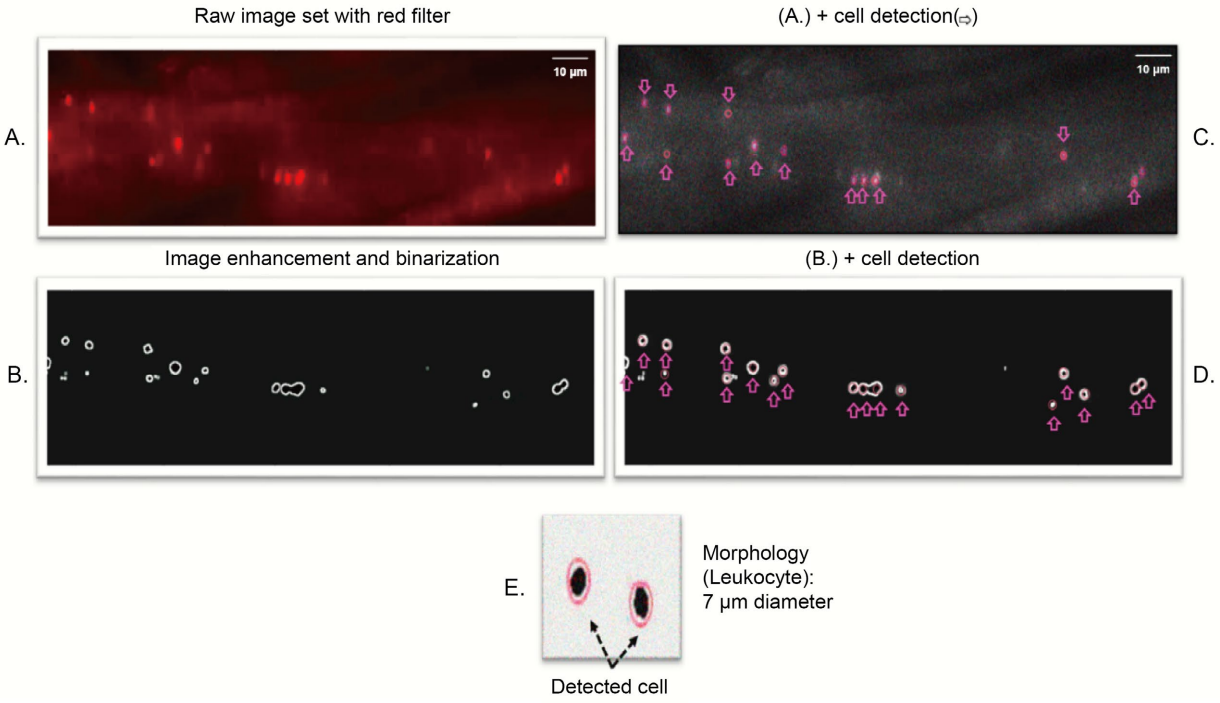

Figure 4. Representative image sets illustrating enhancement, binarization, and cell detection. Time-lapse fluorescence images of leukocytes labeled with R6G were acquired. (A) Initial images were converted to 8-bit and pseudo-colored using a red filter. (B) Images were enhanced and binarized using a custom ImageJ script. Cell detection was performed in TrackMate on both (C) the unenhanced/unbinarized image and (D) the enhanced/binarized image for comparison. (E) Leukocyte detection was achieved using the Laplacian of Gaussian (LoG) spot detection in TrackMate.

Whereas the Kalman filter operated in a two-step process: (1) prediction, estimating a leukocyte's next position based on motion history, and (2) correction, refining that estimate using new, potentially noisy observations. In contrast, the TrackMate LAP tracker included features well-suited for biological imaging, accommodating occlusions, signal fluctuations, and frame-to-frame variability. However, it struggled to accurately track cells transitioning between free-flowing, rolling, adhered states. Free-flowing cells moved at approximately the average blood flow velocity (V_{avg}), rolling cells at velocities between 0 and critical velocity (V_{crit}), where $0 < V_{crit}$, and adhered cells at velocities approaching 0 μm/sec.

2.8.1. Quantifying Leukocyte-Endothelial Interaction from IVM Fluorescent Images

Leukocyte-endothelial interactions, including rolling and adhesion to the venular wall, were assessed following leukocyte flux measurements in the selected venule. Operational definitions of leukocyte flux, rolling, and adherent were are as follows (Table 3).

(A) **Total leukocyte flux:** The total number of leukocytes observed within the observational window including free-flowing, rolling and adhered cells.

(B) **Rolling leukocytes:** Defined by $V_{avg} > 1.0$ μm/sec, but also $V_{avg} < V_{crit}$, persisting for more than 3 frames.

(C) **Adherent leukocytes**: Characterized by $V_{avg} < 1.0$ μm/sec for ≥ 15 frames (~30 sec).

Table 3. Leukocyte classification criteria.

Measure	Criteria 1 (μm/sec)	Criteria 2	Criteria 3
(A) Rolling	Average $V_{xy} > 1.0$	Frames > 3	$V_{max} < V_{crit}$
(B) Adherent	Average $V_{xy} < 1.0$	Frames > 15	Not (A)
(C) Total flux	Not (A)	Not (B)	

2.8.2. Semi-Automatic Leukocyte Tracker (SALT): Modified Lap Tracker

The original LAP tracker was designed for tracking particles moving at a constant velocity but struggled with leukocytes circulating in venules of living animals, where motion conditions are more variable, but also with cells that could drastically shift their velocity between frames (Figure 5). To enhance the accuracy and reliability of leukocyte trajectory prediction, the original TrackMate LAP tracker was modified to utilize a Kalman filter-based multiple-hypothesis tracking model [14, 16, 23] to handle the dynamic leukocyte behavior observed *in vivo*. The Kalman filters model state transitions over time, predicting future positions and refining them using incoming observations and modifying the predictive algorithm real-time based on the cost-penalty-gap functions. As such, with each frame, the algorithm utilized a multi-hypothesis model that was processed in parallel so that for each frame pair $t \to t_{n+1}$, the algorithm would consider (three) possibilities: (A) rolling, (B) adhesion, and or (C) free-flowing (see Table 3 above). The algorithm exemplifies a hybrid AI approach, blending Boolean/Bayesian mathmatics with neural-network-inspired strategies for efficient biomedical image analysis.

After cells were indexed, SALT utilized Kalman filtering integrated with LAP-based optimization to track leukocyte trajectories, utilizing temporal smoothing and prediction mechanisms found in recurrent neural networks (RNNs) or transformers' attention models. While not a traditional deep neural network machine learning framework, SALT utilized unsupervised and semi-supervised functionality to mimic modern deep learning neural network principles in a pseudo-neural network (pseudo-labeling) framework implemented by relatively simplistic tools like ImageJ macros, OpenCV-style plugins, and Excel.

SALT utilized convolutional neural network (CNN) principles in leukocyte detection, recurrent neural network (RNN) principles in leukocyte spatiotemporal movement motion modeling with Kalman filters and

sequence prediction, and finally classification logic that parallels how MLP (multilayer perceptron) layers map features to labels. Modification of the SALT parameters and tracking algorithm were adjusted by comparing predicted trajectories to known leukocyte trajectories obtained from manual frame-by-frame tracking data. The SALT model framework incorporated (Table 4).

A.

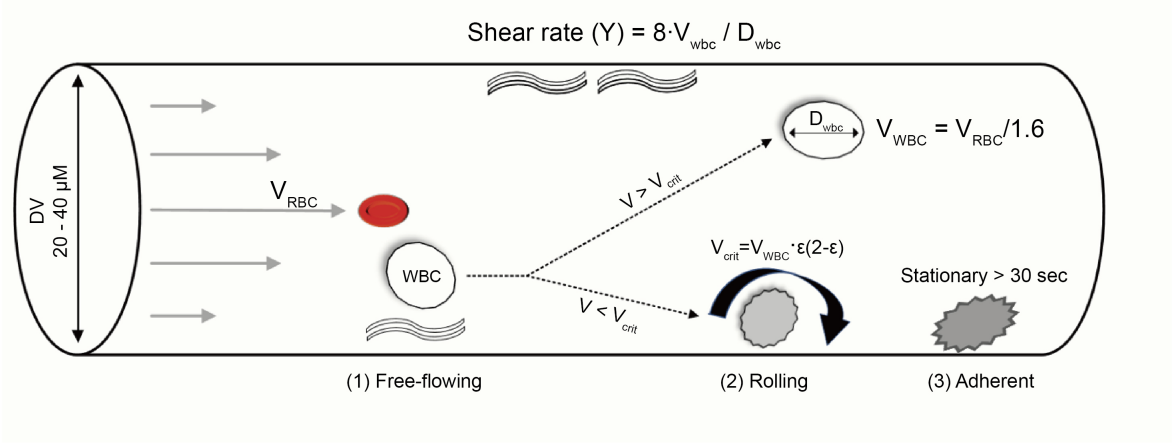

B.

Measure	***Criteria*** 1	***Criteria*** 2	***Criteria*** 3
(A) Rolling	$\overline{V}_{xy}$ ≥ 1.0 *μm/sec*	*Time* ≥ 15 *sec*	$V_{xymax} \le V_{crit}$
(B) Adhesion	$\overline{V}_{xy}$ ≤ 1.0 *μm/sec*	*Time* ≥ 30 *sec*	*Not (A)*
(C) Flux	*Not (A)*	*Not (B)*	

Track	Flux	Rolling	Adhesion
1. (X_1,Y_1)	1	0	1
2. (X_2,Y_2)	1	1	0
3. (X_3,Y_3)	1	0	0
n. (X_i,Y_i)	…	…	…
	$\sum_{i=1}^{n}(Flux)$	$\sum_{i=1}^{n}(Rolling)$	$\sum_{i=1}^{n}(Adhesion)$

Figure 5. Schematic diagram of hemodynamic and leukocyte kinetic assessment. (A) After blood flow velocities and shear rate were quantified as indicated, leukocyte movement status (free-flowing, rolling, and adhering to the wall) was determined based on the definitions described in the Methods 2.8.1 section. (B, left) These criteria were then translated into our working definitions to quantify leukocyte rolling, adhesion, and free-flowing (flux). (B, right) The final Boolean and logical decision array in Excel is shown.

Table 4. Neural networks frameworks adopted by SALT.

SALT Module	Neural Network Equivalent	Function / Purpose
Laplacian of Gaussian (LoG) Filter	Convolutional Layers (e.g., in CNNs)	Detect leukocyte shapes (edge and blob detection)
Kalman Filtering + Linear Assignment (LAP)	Recurrent Networks (RNN/LSTM), Transformers	Predict and refine object positions in sequential data
Conditional Decision Rules (Vavg, Vcrit)	Dense Layers + Softmax / Activation Functions	Classify leukocyte behavior (flowing, rolling, adhered)

1. Prediction of Cell Position (Forward Pass):

Similar to the forward propagation in neural networks, the SALT tracker generated predictions of leukocyte positions based on a priori data (previous frames and leukocyte trajectories). The leukocyte's predicted position was computed using leukocyte free-flowing velocity (V_{avg}) and the threshold for leukocyte

rolling, the critical velocity (V_{crit} This mimics the weighted summation step in neural networks.

2. Cost Function and Penalty System (Loss Function):

The SALT method incorporates a cost function, $f(c)$, similar to the loss function in neural networks, where it computed the penalty based on MSD difference between predicted leukocyte positions and their actual measured positions, represented as,

$$f(c)=\sum\left(x_i-x^*\right)^2\left(t_n\right)+\cdots+\left(x_i-x^*\right)^2\left(t_{n+1}\right) \tag{6}$$

where, x_i was the predicted displacement, and x^* was the actual displacement, quantifying prediction errors, and calculating the loss or error term in a neural network.

3. Adaptive Decision-making (Backpropagation Analogy):

Additionally backpropagation involved adjusting the weights based on errors. In SALT, instead of weight adjustment, the framework updated the leukocyte trajectory prediction dynamically, where each linkage. It employs a Bayesian tracking approach (through MATLAB's μtrack gap function) to refine predictions when leukocytes temporarily disappear from view, effectively adapting future predictions based on past inaccuracies.

4. Multiple-Hypothesis Tracking (Ensemble-like Predictions):

The SALT method uses multiple hypotheses simultaneously to track leukocytes—free-flowing or rolling leukocytes—similar to neural networks utilizing ensemble methods (multiple models and weighted predictions)

2.8.3. Modeling of Leukocyte Kinetics and Training the SALT (Semi-Automated Cell Tracker)

SALT dynamically classifies leukocytes into rolling, adherent, or free-flowing categories based on the blood flow velocity calculations computed for each venule analyzed and the derived threshold velocity (V_{crit}), at which cells start to slow down (rolling) through leukocyte-endothelial interactions, real-time velocity of each , historical data, and the penalty-cost matrices. It combines velocity history with condition-specific predictions (free-flow vs. rolling) to assign the most probable leukocyte trajectory, further resembling how neural networks use historical context and multiple inputs to refine outputs. We adopted a semi-supervised training framework utilizing the blood flow velocity to predict leukocyte free-flowing velocity (V_{avg}) and rolling velocity ($0 < V_{rolling} < V_{crit}$), using the initial search radius (x_i), assuming the cell was free-flowing and the maximal search radius (x_f) to increase the search area to modify the input parameters and fine tune the SALT algorithm. The initial search radius, x_i, was calculated as,

$$f(x_i)=x_0+V_{avg}\cdot t_n \tag{7}$$

where x_0 represents the leukocyte's starting position, V_{avg} is the average leukocyte velocity, and t_n is time. The maximal search radius, x_f, the cell displacement from a predicted position, was calculated as:

$$f(x_f)=V_{crit}\cdot t_n \tag{8}$$

thus, the most probable leukocyte location, $f(x_{i+f})$, combined both radii:

$$f(x_{i+f})=f(x_i)\pm f(x_f) \tag{9}$$

Tracking was initiated with a minimum of three frames, including two consecutive ones. To enhance decision-making, a penalty cost was incorporated into the model by assigning quantitative penalties to suboptimal choices or constraint violations. To ensure accurate linkage between predicted and observed positions, the neural network employed a penalty cost matrix. This cost function was computed based on squared displacement errors between predicted (x_i) and observed positions (x^*):

$$f(c)=\sum_n^{n+1}\left(x_i-x^*\right)^2\left(t_n\right) \tag{10}$$

where x_i represents the predicted displacement and x^* is the true displacement. The greater the

magnitude of the penalty cost, the higher the cost, making the decision less desirable.

To address leukocytes disappearing out of frame or due to image artifacts, we weighted the cost matrix with the gap interval penalty function until the SALT tracking data aligned with the manual ground truth data. For a leukocyte track initiated at frame t_{n-1} and detected through t_n but missing at t_{n+1}, the gap penalty function used estimated the position at t_{n+2} independently of t_{n+1}. The tracking algorithm then retrospectively estimated the missing position at t_{n+1} based on V_{avg}, the LAP algorithm, as:

$$t_{n-1} \to t_n \to \cdots \to t_{n+2} \tag{11}$$

The dots (…) represents the missing gap. If a leukocyte was undetected across successive frames, the penalty cost for the missing gap was estimated based on subsequent linkages; with weights applied according to the gap(s). With each frame-frame link, a cost function determined the most probable trajectory, and was the summation of (penalty cost matrix, gap closing penalty, and probability for the cell to be predicted to be free flowing (Equation (12)) or rolling (Equation (13)). For a predicted track (P), the cost function (C) was conditionally determined by,

$$C_{(x_i)} = P_{\left(C_{x_i}\right)\left(C_{x_f}\right)} f_{(x_i)} \tag{12}$$

$$C_{(x_f)} = P_{\left(C_{x_f}\right)\left(C_{x_i}\right)} f_{(x_f)} \tag{13}$$

where x_i is the predicted position based on initial velocity (assuming leukocyte is free-flowing), x_f is the predicted position based on rolling velocity (slower, transient leukocyte-endothelial interaction, $f_{(x_i)}$ and $f_{(x_f)}$ are the penalty cost functions, and $P\left(C_{x_i} \mid C_{x_f}\right)$ and $P\left(C_{x_f} \mid C_{x_i}\right)$ is the reverse probability that the true cell behavior was governed by the free-flowing trajectory model, x_i, given the evidence from the alternative rolling trajectory model, x_f, and vice versa.

The penalty cost and predicted trajectory was also confined to,

$$C\left(x_i\right) \neq C\left(x_f\right) \text{ over the frames } t_{(n-1)} \leftrightarrow t_{(n)} \leftrightarrow t_{(n+1)} \tag{15}$$

indicating that a cell could only be classified as either rolling or free-flowing for a given frame. The penalty function penalized larger deviations, guiding the algorithm to prefer linkages with minimal spatial displacement error fine-tuned by matching the SALT predicted trajectories while comparing it to the ground truth method. If a leukocyte was undetected across consecutive frames, a cost penalty was applied, terminating the track if it exceeded the predefined threshold ($p < 0.05$) and could not be assigned positions based on predicted trajectories. After fine-tuning the SALT module, the probable trajectories of leukocytes was observed to clean up the noisy detections and yielded greater consistency in the tracking the same cell across frames (**Figure 6**).

2.8.4. Leukocyte Analysis in Excel

After obtaining V_{crit}, V_{avg}, and the number of points, the SALT Tracker computed additional parameters for leukocyte analysis in Excel. The number of adherent and rolling leukocytes were determined off-line from Trackmate data (**Table 3**). The exported variables from the SALT output included *Vxy* (apparent *Vavg*), frames, *Vmin*, *Vmax* and total track duration. These parameters were then input into Excel, where conditional logic formulas quantified the total leukocyte flux, rolling flux, and number of adherent cells for each image set. To validate the SALT method, the image was analyzed in parallel using both SALT and the traditional manual frame-by-frame analysis methods for comparison.

2.9. Statistical Analysis

All statistical analyses were performed using GraphPad Prism 8 (GraphPad Software) and R v4.4.2.

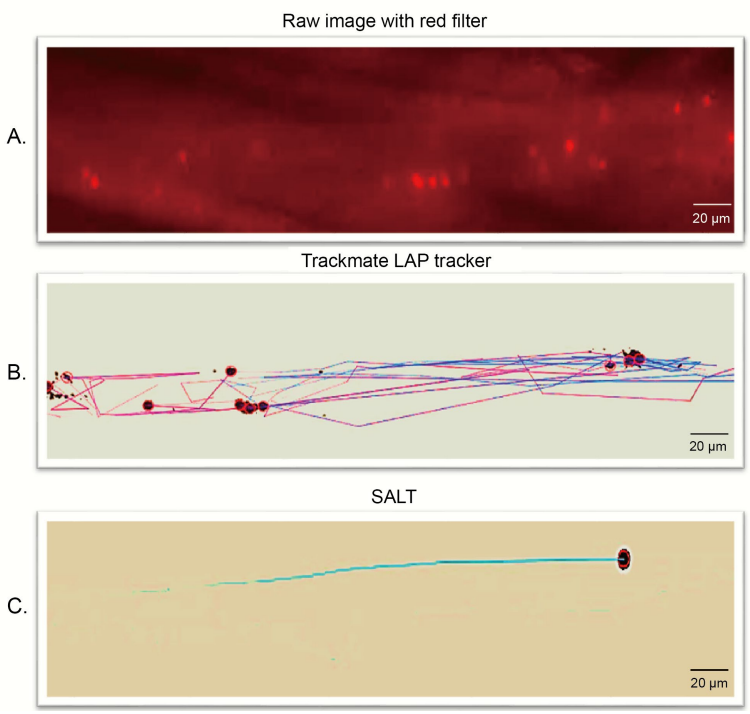

Figure 6. Representative image sets of cell tracking performed by the optimized SALT tracker compared to the Trackmate method. (A) Image stacks were converted to 8-bit and pseudo-colored with a red filter. (B) Predicted tracks were overlaid in ImageJ using the original Trackmate LAP tracker. (C) Predicted tracks was overlaid using the optimized SALT tracker.

Data from multiple experiments (videos) were compiled in Excel spreadsheets and imported into Prism/R for analysis. We first evaluated the relationship between automated SALT measurements and manual measurements using Pearson correlation coefficients (r). High Pearson r values (close to 1.0) indicate strong linear agreement between the two methods. Next, we used paired two-tailed t-tests to determine if there were any systematic differences between SALT and manual measurements (e.g., in average rolling velocity). A significance level of $\alpha = 0.05$ was used throughout; p-values < 0.05 were considered statistically significant. Statistical results are reported in the Results section with exact p-values where relevant. In cases of comparing two groups with potentially unequal variances, Welch's corrected t-test was used instead of the standard t-test. All data are reported as mean ± standard error of the mean (SEM) unless noted otherwise. Normality of distributions was assessed informally.

3. RESULTS

Numerous cell tracking techniques exist [54-57], but most are optimized for *in vitro* analysis and struggle with the challenges of *in vivo* dynamic systems, particularly abrupt cell motion and inter-frame motion distortion. To analyze hemodynamics and quantify leukocyte-endothelial interaction from *in vivo* images, the SALT method was applied. This module used a four-step approach, as outlined:

(A) Vessel Identification and Hemodynamic Parameter Calculation: Identify vessel and determine hemodynamic parameters, as outlined in Table 2, which were essential for computing V_{rbc}, V_{wbc}, V_{crit} using ImageJ.

(B) Image Pre-Processing and Registration: Use a composite template image to remove motion and

background artifacts through image pre-processing and registration.

(C) Leukocyte Tracking with SALT: Apply the customized SALT tracker, which combines template-based leukocytes detection using LoG edge detection and a neural-network-driven spatiotemporal LAP tracker, to detect and track leukocytes.

(D) Quantification of Leukocyte Dynamics: Measure leukocyte flux, rolling, and adhesion using a Boolean conditional framework in Excel.

Tracking leukocytes *in vivo* presents challenges due to their dynamic motion. Free-flowing leukocytes move at average velocities (V_{avg}) ranging from 500 to 10^4 μm/sec, and can transit instantaneously to rolling ($V_{avg} < V_{crit}$) at speeds ranging between 10 to 500 μm/sec, or become adherent and exit the region of interest. While distinguishing between adherent and free-flowing leukocytes was not problematic, accurately tracking a free-flowing leukocyte ($V_x = V_{avg}$) that temporarily rolls ($V_x \le V_{crit}$) or disappears out of the frame was challenging. To address this, the TrackMate LAP tracker was run in parallel with two conditions: [1] $V_{avg} = V_{avg}$ and [2] $V_{avg} = V_{crit}$, along with the MATLAB μtrack frame interval gap cost function. The a priori determination of V_{rbc} allowed for independent prediction of leukocyte movement: $\Delta x_1 = V_{avg} \cdot d(t)$, and $\Delta x_2 = V_{crit} \cdot d(t)$. The LAP tracker, effective for particles moving at constant rates, was enhanced with a pseudo-neural network framework to accommodate leukocyte dynamics. Each cell was tracked as rolling, adherent, or free-flowing (Figure 7).

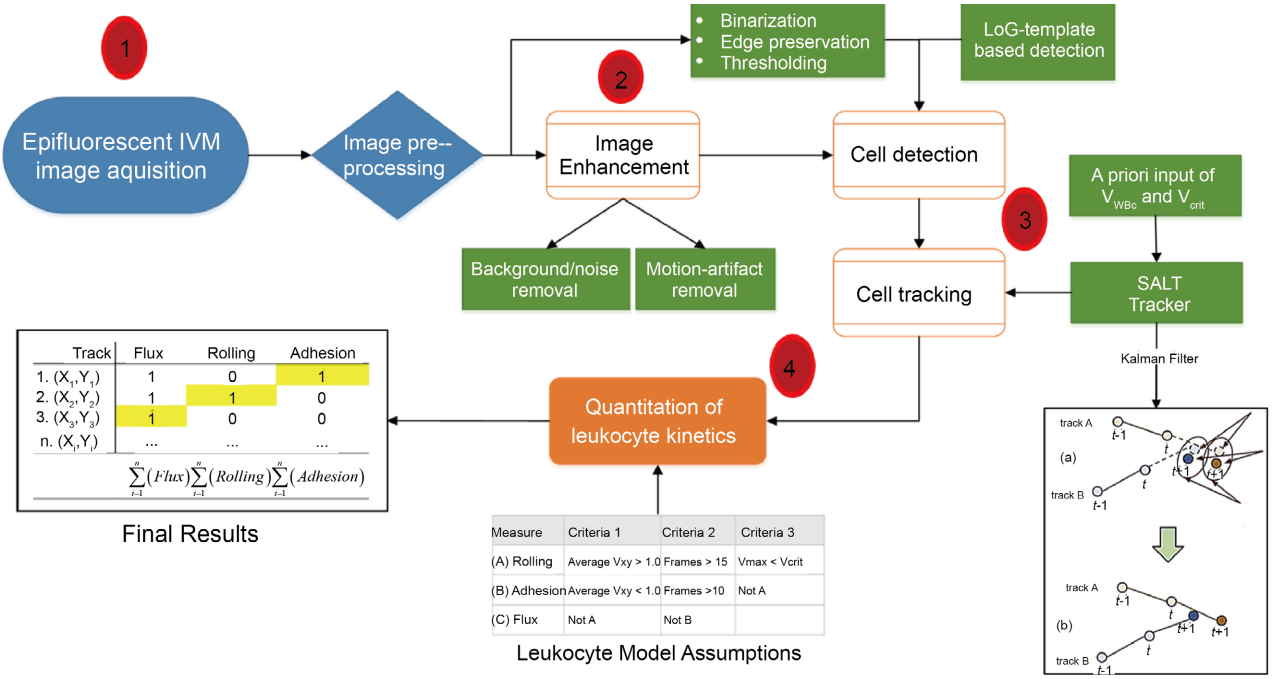

Figure 7. Schematic diagram of SALTfour-step approach to analyze *in vivo* epifluorescent intravital microscopic images, assessing leukocyte-endothelial interaction. Each step is indicated by a red circle. Step 1: Vessel identification and hemodynamic assessment. Step 2: Image enhancement and registration through binarization, edge preservation, and thresholding. Step 3: Leukocyte tracking using the SALT tracker combined with the Kalman filter. Step 4: Quantification of leukocyte flux, rolling, and adhesion using a Boolean framework in Excel. For the Kalman filter tracker (bottom right), the predicted positions for each time point [$track\ A_{(t_1,t,t_{+1})}$, $track\ B_{(t_{-1},t,t_{+1})}$] (a) are determined by two kalman predictive algorithms and compared to actual measured positions. The measured positions are then linked to the predicted positions based on mean square displacement (b), resulting in a best estimate of the predicted position.

The SALT method demonstrated robustness and optimization using a priori parameters for varying conditions, minimizing subjective bias. All parameters assessed showed statistical significance, with no significant deviations in comparisons to manual tracking or inexperienced users. The SALT method exhibited high inter- and intra-rater validity and is suitable for future intravital microscopy (IVM) image analysis. Further validation under inflammatory conditions and benchmarking against IEEE dataset comparisons would strengthen the model's applicability, though incorporating optical flow estimation of V_{rbc} may increase cost and complexity.

In this study, leukocyte blood flow velocity (V_{wbc}) was estimated from the centerline blood flow velocity (V_{rbc}) using an empirical correction factor of 1.67. To ensure the accuracy of the computed blood flow velocity (V_{xy}), V_{wbc} was manually calculated by tracking leukocytes frame-to-frame in epifluorescent images and compared to V_{xy} derived from optical flow. The comparison yielded an empirical factor of 1.67 ± 0.06, consistent with previously reported *in vivo* cremaster microvascular blood flow velocity ($p < 0.001$) [45, 51].

3.1. Validation of the SALT Tracker

To validate SALT, an expert (Rater 1) and two novices (Raters 2 and 3) independently analyzed images using both SALT and manual tracking methods. Leukocyte rolling velocity was assessed as described below in Table 5.

Table 5. SALT validation methodology.

Structured Comparison	N	Rater (# of cells analyzed)[a]
Manual vs SALT	5	Manual Rater 1[b] (318 cells) vs SALT Rater 1 (283 cells)
SALT vs SALT	8	Rater 1 (322 cells) vs Rater 2[b] (303 cells) and Rater 3[b] (235 cells)

[a]represents the # of cells analyzed. [b]indicates rater designations: Rater 1 (expert), Rater 2 (novice 1), Rater 3 (novice 2).

To determine cell-to-cell precision in tracking, individual leukocytes rolling velocity was cross-analyzed on image sets, comparing data obtained from the SALT method ($n = 5$, 283 cells) against the ground truth ($n = 5$, 318 cells). RMSE values, expressed as either standard error in microns or percentages, with lower values reflecting higher precision and centroid trackers having RMSE values upwards of 66.8% [58]. Cui (2006) created a Monte Carlo approach to rolling leukocyte tracking *in vivo* and assessed a centroid tracker, correlation tracker, GVF snake tracker, and Monte Carlo tracker, for rolling leukocyte analysis, yielding RMSE values of 1.04 μm, 0.97 μm, 0.52 μm, and 0.47 μm, respectively [59].

For intra-rater validity assessment, a single rater (Rater 1) analyzed leukocyte rolling velocity ($n = 5$) using both SALT (283 cells) and manual (318 cells) tracking methods. Minimal deviation was observed (RMSE = 0.11 μm/sec, 1.92%) between SALT (7.95 ± 2.1 μm/sec, $n = 5$) and manual tracking (7.8 ± 5.1 μm/sec, $n = 5$), further exhibiting a very high correlation between SALT and manual tracking measure ($r = 0.97$, $p < 0.001$) (**Figure 8, left**).

For inter-rater validity evaluation, leukocyte rolling velocity data (n = 8) was analyzed in parallel by 3 raters: Rater 1 (322 cells), and 2 novice raters, Rater 2 (303 cells) and Rater 3 (235 cells) (**Figure 8, right**). Comparing leukocyte rolling RMSE of 1.13 μm/sec (9.88%) between novice raters (8.1 ± 3.4 μm/sec; $n = 8$) and the expert rater (6.50 ± 1.20 μm/sec; $n = 8$) was observed. The correlation was $r = 0.89$ ($p = 0.055$). Although the correlation was strong, it was near statistical significance likely due to individual cell tracking differences between raters. Welch's t-test ($t = 0.0083$, $p = 0.993$) indicated no significant difference in leukocyte rolling velocity between these two approaches when accounting for heterogenic populations (see **Abbreviations**).

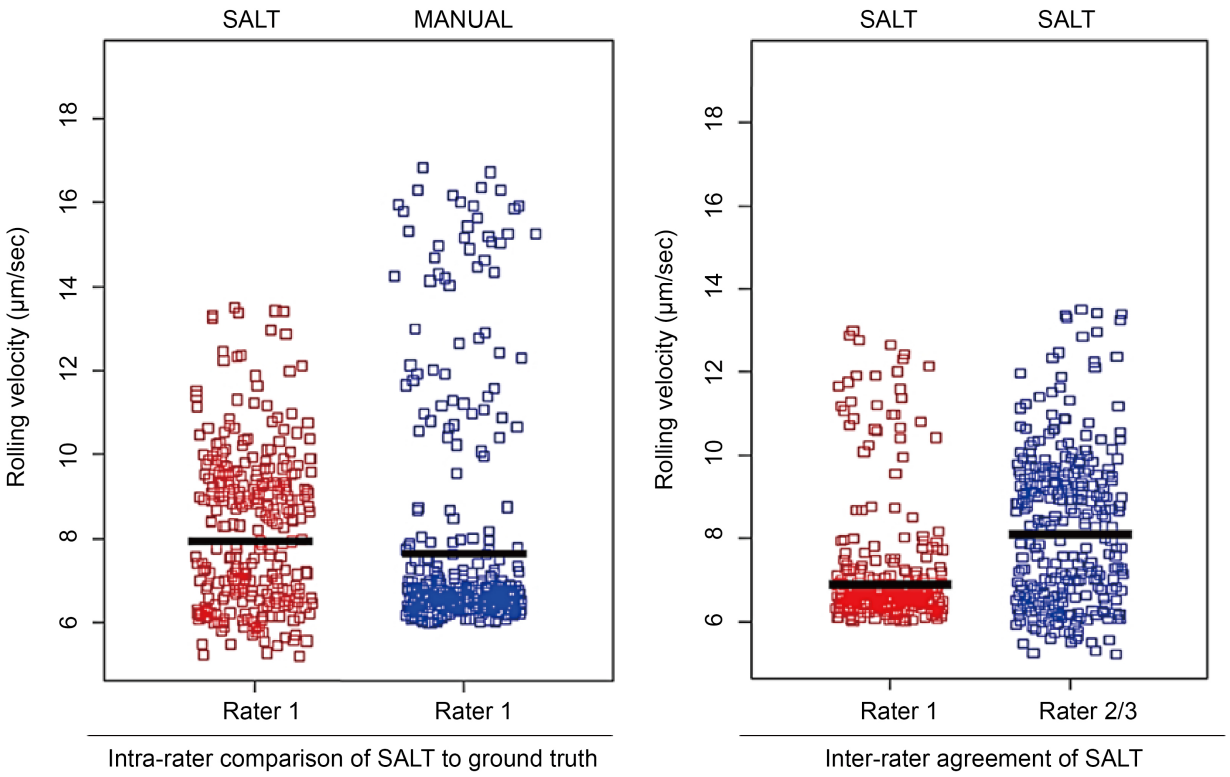

Figure 8. **Intra-rater and inter-rater analyses of leukocyte rolling velocity were conducted to validate the SALT module compared to the manual frame-by fame cell tracking method, considered the "ground truth" Left: Rater 1 assessed leukocyte rolling velocity from images acquired from individual experiments ($n = 5$) using the SALT (7.95 ± 2.10 µm/sec) and the manual frame-by-frame (7.80 ± 5.10 µm/sec) methods. Right: Images from eight experiments ($n = 8$) were independently analyzed by Rater 1 (expert; 6.50 ± 1.20 µm/sec) and Rater 2 & 3 (novices; 8.10 ± 3.40 µm/sec) using SALT method. Red: Salt method; Blue: Manual method. There was no difference between SALT and manual methods for both intra-rater and inter-rater validity ($p < 0.05$).**

3.2. Leukocyte-Endothelial Interaction Using the SALT Method

In addition to leukocyte rolling velocity to define local tracking accuracy as described in Section 3.1, the quantification of leukocyte-endothelium interactions-such as leukocyte displacement, total leukocyte flux, rolling flux, and adherent cells was assessed to further validate the accuracy of the SALT module ($n = 8$) vs ground truth, manual frame-by-frame tracking ($n = 8$), and were measured at 0, 5, 10, 15, 30, 45, 60 minutes in mice under resting conditions, shown in **Figure 9**.

The Pearson correlation coefficient (r) was calculated to assess the relationship between data obtained from SALT and manual (ground truth) analyses [58] shown in **Figure 9**, insets and summarized in **Table 5**. For each variable measured at each time point, denoted as X_n and Y_n, respectively, the correlation was computed:

$$\text{Predicted}\left(X_n, Y_n\right) = \text{Manual}\left(X_n, Y_n\right) \tag{14}$$

If SALT accurately predicted leukocyte movement, each measured variable would have a perfectly linear relationship ($r = 1$), as assessed by Pearson's correlation coefficient

Comparisons of leukocyte flux, rolling, and adherence using SALT versus manual ground truth analysis across multiple experiments yielded consistently strong correlations (**Table 5**). Total leukocyte flux, rolling

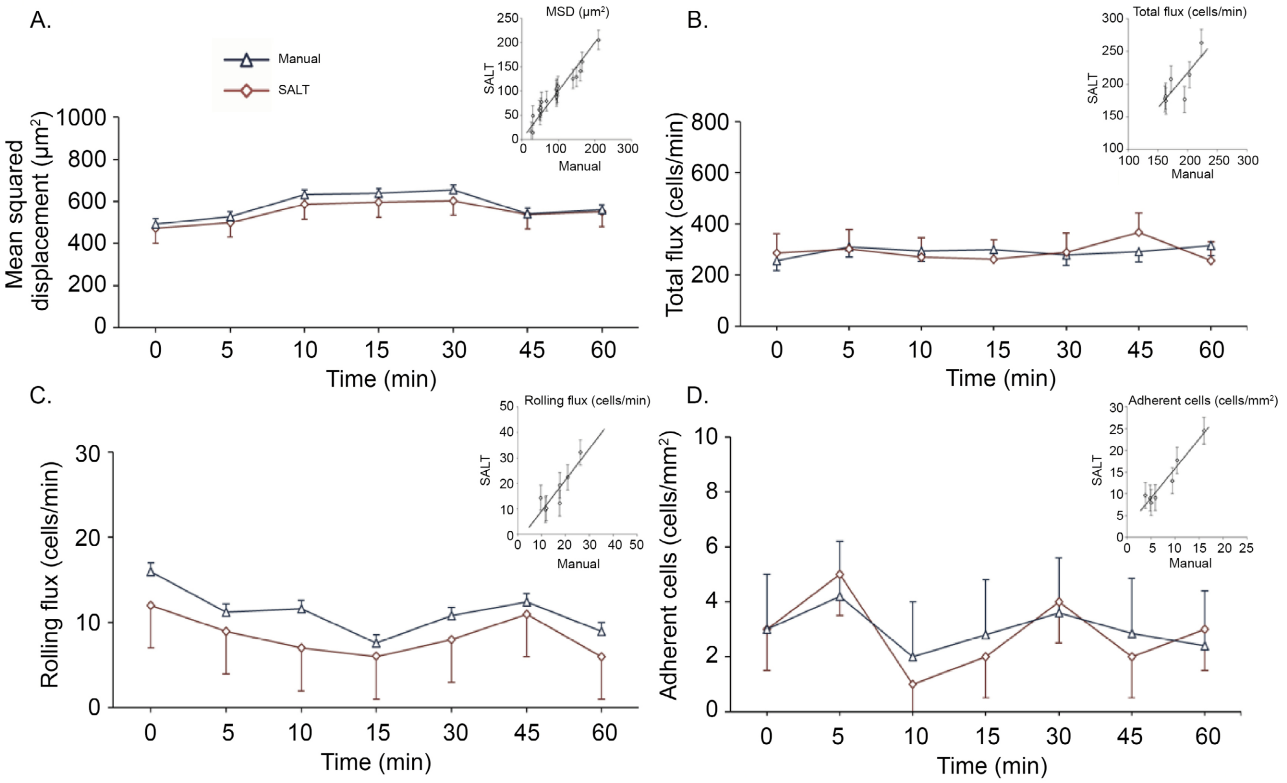

Figure 9. Validation of the SALT module by assessing basal leukocyte kinetics over 60 mins. Data obtained from image analysis using the SALT method were compared to manual analysis (n = 6). (A) Mean square displacement (MSD, 100 μm²) of the leukocyte tracks, (B) leukocyte total flux (number of cells/min), (C) rolling leukocyte flux (number of rolling cells/min), and (D)adherent cells (number of adherent cells / 100 μm) were assessed. Three independent assessments were conducted across eighteen different sites of the venule. Representative plots with mean ± 95% confidence interval are shown. Graph insets display the correlation between predicted (SALT) and manual analysis (ground truth) analyses.

flux, and adherent leukocyte counts demonstrated significant correlation coefficients, r = 0.81, 0.89, and 0.97, respectively ($p < 0.05$). Hemodynamic-dependent parameters including leukocyte rolling velocity and leukocyte displacement, the mean squared displacement (MSD), and wall shear rate (γ_W), exhibited strong relationships with blood flow velocity highlighting SALT's reliability in dynamic vascular environments, r = 0.97, 0.96, and 0.98, respectively ($p < 0.001$) (Table 6).

Table 6. Correlation of SALT and with respective manual ground truth parameters.

Parameters	r	SEr	T-test	Sig
Leukocyte kinetics				
Total leukocyte flux	0.81	0.24	3.38	*
Rolling leukocyte flux	0.89	0.19	4.69	*
Adherent cells / 100 μm	0.97	0.10	9.68	**

Continued

Hemodynamic-dependent				
Rolling V_{WBC}	0.97	0.10	10.20	**
Leukocyte MSD	0.96	0.11	13.45	**
Wall shear rater (γ_W)	0.98	0.09	11.20	**

Pearson correlation coefficient (r), mean squared displacement (MSD), Standard error (SEr), *p < 0.05, **p < 0.001.

Although, total leukocyte flux and rolling flux showed a slightly weaker association, with r values of 0.81 and 0.89, respectively, both were statistically significant ($p < 0.05$). No significant changes were observed in leukocyte displacement, total leukocyte flux, rolling flux, and adherent cell counts over the 60-minute analysis period (**Figure 9**). To confirm that hemodynamics were not influencing any observed differences or variance, both hemodynamic-dependent and hemodynamic-independent parameters associated with leukocyte-endothelial interaction were included in the analysis (**Table 6**) [6, 8, 13, 40, 42, 45, 60-62].

3.3. Comparison of Computational Cost of SALT vs Other Tracking Methods

The computational cost in cell tracking, primarily refers to the time, resources, and complexity involved in processing and analyzing image data for leukocyte tracking. The SALT method, developed for semi-automatic leukocyte tracking *in vivo*, explicitly aimed to address the computational costs associated with manual frame-by-frame analysis, which is typically time-consuming and labor-intensive, and to maximize computational efficiency (**Table 7**).

Table 7. Computational cost comparison between SALT and other tracking methods.

Parameter	Trackers Employed		
	Manual	TrackMate	SALT
Time per Dataset	~1.5 - 2 hrs	~20 - 30 mins	~5 - 7 mins
RMSE (vs Manual)	N/A	High	Low (1% - 10%)
Accuracy (r)	Ground truth	<0.7 typical	0.96 - 0.98
Cost Function	N/A	Simple	Yes (Kalman + Bayesian)
Runtime Adaptation	None	Static	Dynamic

4. DISCUSSION

We develop a novel cell-tracking method specifically designed to assess hemodynamics and leukocyte-endothelial interactions by analyzing *in vivo* microcirculation images using ImageJ. Traditional manual tracking methods pose significant challenges, primarily due to (1) excessive time consumption and (2) inconsistency between image analysts, despite being considered the "ground truth". To our knowledge, the SALT module is the first method utilizing ImageJ, an open-source NIH software, to track leukocytes in circulating blood from images captured in living animals.

Tracking leukocytes in the dynamic *in vivo* microcirculation presents significant challenges, resulting in false positive or false negative. The tracked cells disappear from the region of interest (ROI), leading to false negatives, due to several factors. The biological factors include abrupt cell transition between free-flowing, rolling, and adhesion and cell extravasation. Free-flowing leukocytes move at velocities of 500-1,000

μm/sec [13] but can rapidly slow to rolling ($V_{wbc} < V_{crit}$) or become fully adherent to the vascular endothelium. Imaging and optical limitations encompass cells moved out of the focal plan due to hemodynamic forces. In contrast, inconsistent pixel intensity across frames of the image stack due to respiratory motion artifacts can result in false positives.

To address these challenges, we modified the TrackMate LAP tracker by integrating MATLAB's μtrack gap cost function, applied in parallel under two conditions ($V_{wbc} = V_{avg}$ and $V_{wbc} = V_{crit}$). This modification significantly improved tracking accuracy, particularly for transient rolling behaviors.

SALT demonstrated substantial improvements in efficiency, accuracy, and reproducibility compared to manual tracking and TrackMate alone. By integrating optical flow algorithms (FlowJ and PIV) with a modified TrackMate framework, SALT maintained precision under complex hemodynamic conditions while dramatically reducing analysis time—from hours per dataset (manual tracking) to minutes.

Validation against manual tracking, the current "gold standard", confirmed accuracy of SALT module, with high correlation and low RMSE values indicating minimal deviation. Additionally, low variability between novice and expert users highlighted SALT's reproducibility and user independence.

Despite these advantages, minor discrepancies in total leukocyte flux were observed, likely due to subtle differences in defining rolling versus free-flowing cells, consistent with previous automated tracking (14). However, SALT's innovative integration of hemodynamic parameters (V_{avg}, V_{crit}) into the tracking decision framework substantially mitigated these inconsistences. Regarding efficiency, SALT significantly streamlined image analysis time, reducing the required time for analysis by approximately 60-75% compared to manual tracking while enhancing reproducibility by minimizing human observer variability and bias.

Designed to enhance *in vivo* image analysis for leukocyte-endothelial interactions studies, SALT provides a balance of accuracy, computational efficiency, and ease of use. It demonstrated high inter-rater and intra-rater reliability for rolling velocity, correlating strongly with manual methods. These findings highlight the method's accuracy and reliability, representing a significant advancement in the field of leukocyte tracking. SALT is expected to serve as a foundation for the development of automated methods for *in vivo* microcirculatory leukocyte tracking, leveraging advancements in artificial intelligence. This innovation has the potential to enhance our understanding of leukocyte dynamics and their role in inflammatory processes, paving the way for more effective therapeutic strategies.

ACKNOWLEDGEMENTS

The authors acknowledge funding support from Missouri State University and the Department of Biomedical Sciences. We sincerely thank Corynn Knight for valuable discussions on image analysis techniques and Rebecca Allen for her assistance in ordering supplies and reagents.

CONFLICTS OF INTEREST

The authors declare no conflicts of interest regarding the publication of this paper.

REFERENCES

1. Pettersson, U.S., Christoffersson, G., Massena, S., Ahl, D., Jansson, L., Henriksnäs, J., *et al.* (2011) Increased Recruitment but Impaired Function of Leukocytes during Inflammation in Mouse Models of Type 1 and Type 2 Diabetes. *PLOS ONE*, **6**, e22480. https://doi.org/10.1371/journal.pone.0022480
2. Yayan, J. (2013) Emerging Families of Biomarkers for Coronary Artery Disease: Inflammatory Mediators. *Vascular Health and Risk Management*, **9**, 435-456. https://doi.org/10.2147/vhrm.s45704
3. Vitiello, L., Spoletini, I., Gorini, S., Pontecorvo, L., Ferrari, D., Ferraro, E., *et al.* (2014) Microvascular Inflammation in Atherosclerosis. *IJC Metabolic & Endocrine*, **3**, 1-7. https://doi.org/10.1016/j.ijcme.2014.03.002
4. Haq, S., Grondin, J., Banskota, S. and Khan, W.I. (2019) Autophagy: Roles in Intestinal Mucosal Homeostasis and Inflammation. *Journal of Biomedical Science*, **26**, Article No. 19. https://doi.org/10.1186/s12929-019-0512-2

5. Arendshorst, W.J., Bell, P.D., Bhattacharya, J., Bohlen, H.G., Breslin, J.W., Carey, R.M. *et al.* (2008) Handbook of Physiology: Microrcirculation. American Physiological Society.

6. Granger, D.N. and Kubes, P. (1994) The Microcirculation and Inflammation: Modulation of Leukocyte-Endothelial Cell Adhesion. *Journal of Leukocyte Biology*, **55**, 662-675. https://doi.org/10.1002/jlb.55.5.662

7. Bienvenu, K. and Granger, D.N. (1993) Molecular Determinants of Shear Rate-Dependent Leukocyte Adhesion in Postcapillary Venules. *American Journal of Physiology-Heart and Circulatory Physiology*, **264**, H1504-H1508. https://doi.org/10.1152/ajpheart.1993.264.5.h1504

8. Chapman, G.B. and Cokelet, G.R. (1997) Model Studies of Leukocyte-Endothelium-Blood Interactions. *Biorheology*, **34**, 37-56. https://doi.org/10.3233/bir-1997-34103

9. Langer, H.F. and Chavakis, T. (2009) Leukocyte—Endothelial Interactions in Inflammation. *Journal of Cellular and Molecular Medicine*, **13**, 1211-1220. https://doi.org/10.1111/j.1582-4934.2009.00811.x

10. da Silva, B.C.G., Ferrari, R.J. and Tavares, J.C. (2015) Detection of Leukocytes in Intravital Video Microscopy Based on the Analysis of Hessian Matrix Eigenvalues. 2015 28*th SIBGRAPI Conference on Graphics, Patterns and Images*, Salvador, 26-29 August 2015, 345-352. https://doi.org/10.1109/sibgrapi.2015.48

11. Grădinaru, C., Łopacińska, J.M., Huth, J., Kestler, H.A., Flyvbjerg, H. and Mølhave, K. (2012) Assessment of Automated Analyses of Cell Migration on Flat and Nanostructured Surfaces. *Computational and Structural Biotechnology Journal*, **1**, e201207004. https://doi.org/10.5936/csbj.201207004

12. Xu, N., Lei, X. and Liu, L. (2011) Tracking Neutrophil Intraluminal Crawling, Transendothelial Migration and Chemotaxis in Tissue by Intravital Video Microscopy. *Journal of Visualized Experiments*, **55**, e3296. https://doi.org/10.3791/3296

13. Sperandio, M., Pickard, J., Unnikrishnan, S., Acton, S.T. and Ley, K. (2006) Analysis of Leukocyte Rolling *in Vivo* and *in Vitro*. *Methods in Enzymology*, **416**, 346-371. https://doi.org/10.1016/s0076-6879(06)16023-1

14. Ray, N., Acton, S.T. and Ley, K. (2002) Tracking Leukocytes *in Vivo* with Shape and Size Constrained Active Contours. *IEEE Transactions on Medical Imaging*, **21**, 1222-1235. https://doi.org/10.1109/tmi.2002.806291

15. Lagrange, J., Kossmann, S., Kiouptsi, K. and Wenzel, P. (2018) Visualizing Leukocyte Rolling and Adhesion in Angiotensin II-Infused Mice: Techniques and Pitfalls. *Journal of Visualized Experiments*, **131**, e56948. https://doi.org/10.3791/56948

16. Klyscz, T., Jünger, M., Jung, F. and Zeintl, H. (1997) Cap Image—Ein Neuartiges Computerunterstütztes Videobildanalysesystem Für Die Dynamische Kapillarmikroskopie—Cap Image—A Newly-Developed Computer-Aided Videoframe Analysis System for Dynamic Capillaroscopy. *Biomedizinische Technik/Biomedical Engineering*, **42**, 168-175. https://doi.org/10.1515/bmte.1997.42.6.168

17. Dunne, J.L., Goobic, A.P., Acton, S.T. and Ley, K. (2004) A Novel Method to Analyze Leukocyte Rolling Behavior *in Vivo*. *Biological Procedures Online*, **6**, 173-179. https://doi.org/10.1251/bpo87

18. Anders, X., Zhang, C. and Yuan, H. (2006). Automatic Intravital Video Mining of Rolling and Adhering Leukocytes. 2006 5*th International Conference on Machine Learning and Applications* (*ICMLA*'06), Orlando, 14-16 December 2006, 174-179. https://doi.org/10.1109/icmla.2006.18

19. Zhang, C., Chen, W., Yang, L. and Chen, X. (2007) Detection of Leukocytes from *in Vivo* Videos. *The* 2007 *International Conference on Intelligent Pervasive Computing* (*IPC* 2007), Jeju, 11-13 October 2007, 68-71. https://doi.org/10.1109/ipc.2007.19

20. Sacan, A., Ferhatosmanoglu, H. and Coskun, H. (2008) CellTrack: An Open-Source Software for Cell Tracking and Motility Analysis. *Bioinformatics*, **24**, 1647-1649. https://doi.org/10.1093/bioinformatics/btn247

21. Huang, T., Lin, W., Wu, C., Zhang, G. and Lin, K. (2010) Experimental Estimation of Blood Flow Velocity through

Simulation of Intravital Microscopic Imaging in Micro-Vessels by Different Image Processing Methods. *Microvascular Research*, **80**, 477-483. https://doi.org/10.1016/j.mvr.2010.07.007

22. Klein, J., Leupold, S., Biegler, I., Biedendieck, R., Münch, R. and Jahn, D. (2012) TLM-Tracker: Software for Cell Segmentation, Tracking and Lineage Analysis in Time-Lapse Microscopy Movies. *Bioinformatics*, **28**, 2276-2277. https://doi.org/10.1093/bioinformatics/bts424
23. Chalfoun, J., Majurski, M., Dima, A., Halter, M., Bhadriraju, K. and Brady, M. (2016) Lineage Mapper: A Versatile Cell and Particle Tracker. *Scientific Reports*, **6**, Article No. 36984. https://doi.org/10.1038/srep36984
24. Jaqaman, K., Loerke, D., Mettlen, M., Kuwata, H., Grinstein, S., Schmid, S.L., *et al.* (2008) Robust Single-Particle Tracking in Live-Cell Time-Lapse Sequences. *Nature Methods*, **5**, 695-702. https://doi.org/10.1038/nmeth.1237
25. Kan, A., Chakravorty, R., Bailey, J., Leckie, C., Markham, J. and Dowling, M.R. (2011) Automated and Semi-Automated Cell Tracking: Addressing Portability Challenges. *Journal of Microscopy*, **244**, 194-213. https://doi.org/10.1111/j.1365-2818.2011.03529.x
26. Chen, Y., Zhao, Z., Liu, L. and Li, H. (2011) Automatic Tracking and Measurement of the Motion of Blood Cells in Microvessels Based on Analysis of Multiple Spatiotemporal Images. *Measurement Science and Technology*, **22**, Article ID: 045803. https://doi.org/10.1088/0957-0233/22/4/045803
27. Baez, S. (1973) An Open Cremaster Muscle Preparation for the Study of Blood Vessels by *in Vivo* Microscopy. *Microvascular Research*, **5**, 384-394. https://doi.org/10.1016/0026-2862(73)90054-x
28. Damiano, E.R., Westheider, J., Tözeren, A. and Ley, K. (1996) Variation in the Velocity, Deformation, and Adhesion Energy Density of Leukocytes Rolling within Venules. *Circulation Research*, **79**, 1122-1130. https://doi.org/10.1161/01.res.79.6.1122
29. Norman, K., Moore, K., McEver, R. and Ley, K. (1995) Leukocyte Rolling *in Vivo* Is Mediated by P-Selectin Glycoprotein Ligand-1. *Blood*, **86**, 4417-4421. https://doi.org/10.1182/blood.v86.12.4417.bloodjournal86124417
30. Granger, D.N. and Senchenkova, E. (2010) Inflammation and the Microcirculation. *Colloquium Series on Integrated Systems Physiology*: *From Molecule to Function*, **2**, 1-87. https://doi.org/10.4199/c00013ed1v01y201006isp008
31. Gavins, F.N.E. and Chatterjee, B.E. (2004) Intravital Microscopy for the Study of Mouse Microcirculation in Anti-Inflammatory Drug Research: Focus on the Mesentery and Cremaster Preparations. *Journal of Pharmacological and Toxicological Methods*, **49**, 1-14. https://doi.org/10.1016/s1056-8719(03)00057-1
32. D. Edelstein, A., A. Tsuchida, M., Amodaj, N., Pinkard, H., D. Vale, R. and Stuurman, N. (2014) Advanced Methods of Microscope Control Using Mmanager Software. *Journal of Biological Methods*, **1**, Article 1. https://doi.org/10.14440/jbm.2014.36
33. Goobic, A.P., Tang, J. and Acton, S.T. (2005) Image Stabilization and Registration for Tracking Cells in the Microvasculature. *IEEE Transactions on Biomedical Engineering*, **52**, 287-299. https://doi.org/10.1109/tbme.2004.840468
34. Guo, D.M., van de Ven, A.L. and Xiaobo Zhou, (2014) Red Blood Cell Tracking Using Optical Flow Methods. *IEEE Journal of Biomedical and Health Informatics*, **18**, 991-998. https://doi.org/10.1109/jbhi.2013.2281915
35. Gonzalez, R. and Woods, R. (2008) Digital Image Processing. 3rd Edition, Prentice Hall.
36. Grimes, W. (2016) Image Processing and Analysis Methods in Quantitative Endothelial Cell Biology. Master's Thesis, University College London.
37. Sahoo, P., Wilkins, C. and Yeager, J. (1997) Threshold Selection Using Renyi's Entropy. *Pattern Recognition*, **30**, 71-84. https://doi.org/10.1016/s0031-3203(96)00065-9

38. Tinevez, J., Perry, N., Schindelin, J., Hoopes, G.M., Reynolds, G.D., Laplantine, E., *et al.* (2017) Trackmate: An Open and Extensible Platform for Single-Particle Tracking. *Methods*, **115**, 80-90. https://doi.org/10.1016/j.ymeth.2016.09.016

39. Adrian, R.J. and Westerweel, J. (2011) Particle Image Velocimetry. Springer. https://doi.org/10.1007/978-3-540-72308-0

40. Pittman, R.N. and Ellsworth, M.L. (1986) Estimation of Red Cell Flow in Microvessels: Consequences of the Baker-Wayland Spatial Averaging Model. *Microvascular Research*, **32**, 371-388. https://doi.org/10.1016/0026-2862(86)90072-5

41. Tang, J., Ley, K.F. and Hunt, C.A. (2007) Dynamics of in Silico Leukocyte Rolling, Activation, and Adhesion. *BMC Systems Biology*, **1**, Article No. 14. https://doi.org/10.1186/1752-0509-1-14

42. Jain, R.K., Munn, L.L. and Fukumura, D. (2013) Measuring Leukocyte-Endothelial Interactions in Mice. *Cold Spring Harbor Protocols*, No. 6, 561-563. https://doi.org/10.1101/pdb.prot075085

43. Gregório, B.C., Silva, D., Ferrari, R.J. and Carvalho-Tavares, J. (2011) Automated Technique for *in Vivo* Analysis of Leukocyte Recruitment of Mice Brain Microcirculation. John Wiley & Sons, Inc.

44. Firrell, J.C. and Lipowsky, H.H. (1989) Leukocyte Margination and Deformation in Mesenteric Venules of Rat. *American Journal of Physiology-Heart and Circulatory Physiology*, **256**, H1667-H1674. https://doi.org/10.1152/ajpheart.1989.256.6.h1667

45. Ley, K. and Gaehtgens, P. (1991) Endothelial, Not Hemodynamic, Differences Are Responsible for Preferential Leukocyte Rolling in Rat Mesenteric Venules. *Circulation Research*, **69**, 1034-1041. https://doi.org/10.1161/01.res.69.4.1034

46. Lipowsky, H.H., Kovalcheck, S. and Zweifach, B.W. (1978) The Distribution of Blood Rheological Parameters in the Microvasculature of Cat Mesentery. *Circulation Research*, **43**, 738-749. https://doi.org/10.1161/01.res.43.5.738

47. Eden, E., Waisman, D., Rudzsky, M., Bitterman, H., Brod, V. and Rivlin, E. (2005) An Automated Method for Analysis of Flow Characteristics of Circulating Particles from *in Vivo* Video Microscopy. *IEEE Transactions on Medical Imaging*, **24**, 1011-1024. https://doi.org/10.1109/tmi.2005.851759

48. Ghosh, M., Das, D.K., Ray, A.K. and Chakraborty, C. (2011) Development of Renyi's Entropy Based Fuzzy Divergence Measure for Leukocyte Segmentation. *Journal of Medical Imaging and Health Informatics*, **1**, 334-340. https://doi.org/10.1166/jmihi.2011.1052

49. Wu, C., Zhang, G., Huang, T. and Lin, K. (2009) Red Blood Cell Velocity Measurements of Complete Capillary in Finger Nail-Fold Using Optical Flow Estimation. *Microvascular Research*, **78**, 319-324. https://doi.org/10.1016/j.mvr.2009.07.002

50. Arora, A. and Qazi, T. (2014) Computer Vision Based Tracking of Biological Cells—A Review. *International Conference of Advance Research and Innovation*, Seville, 17-19 November 2014, 118-126.

51. Barron, J.L., Fleet, D.J. and Beauchemin, S.S. (1994) Performance of Optical Flow Techniques. *International Journal of Computer Vision*, **12**, 43-77. https://doi.org/10.1007/bf01420984

52. Sato, Y., Chen, J., Zoroofi, R.A., Harada, N., Tamura, S. and Shiga, T. (1997) Automatic Extraction and Measurement of Leukocyte Motion in Microvessels Using Spatiotemporal Image Analysis. *IEEE Transactions on Biomedical Engineering*, **44**, 225-236. https://doi.org/10.1109/10.563292

53. Stuurman, N. and Swedlow, J.R. (2011) Software Tools, Data Structures, and Interfaces for Microscope Imaging. *Cold Spring Harbor Protocols*, No. 1, 50-61. https://doi.org/10.1101/pdb.top067504

54. Maška, M., Ulman, V., Svoboda, D., Matula, P., Matula, P., Ederra, C., *et al.* (2014) A Benchmark for Comparison of Cell Tracking Algorithms. *Bioinformatics*, **30**, 1609-1617. https://doi.org/10.1093/bioinformatics/btu080

55. Meijering, E., Dzyubachyk, O. and Smal, I. (2012) Methods for Cell and Particle Tracking. *Methods in Enzymology*, **504**, 183-200. https://doi.org/10.1016/b978-0-12-391857-4.00009-4

56. Kan, A., Chakravorty, R., Bailey, J., Leckie, C., Markham, J. and Dowling, M.R. (2011) Automated and Semi-Automated Cell Tracking: Addressing Portability Challenges. *Journal of Microscopy*, **244**, 194-213. https://doi.org/10.1111/j.1365-2818.2011.03529.x

57. Chenouard, N., Smal, I., de Chaumont, F., Maška, M., Sbalzarini, I.F., Gong, Y., *et al.* (2014) Objective Comparison of Particle Tracking Methods. *Nature Methods*, **11**, 281-289. https://doi.org/10.1038/nmeth.2808

58. Acton, S.T., Wethmar, K. and Ley, K. (2002) Automatic Tracking of Rolling Leukocytes *in Vivo*. *Microvascular Research*, **63**, 139-148. https://doi.org/10.1006/mvre.2001.2373

59. Cui, J., Acton, S.T. and Lin, Z. (2006) A Monte Carlo Approach to Rolling Leukocyte Tracking *in Vivo*. *Medical Image Analysis*, **10**, 598-610. https://doi.org/10.1016/j.media.2006.05.006

60. Chatzizisis, Y.S., Coskun, A.U., Jonas, M., Edelman, E.R., Feldman, C.L. and Stone, P.H. (2007) Role of Endothelial Shear Stress in the Natural History of Coronary Atherosclerosis and Vascular Remodeling. *Journal of the American College of Cardiology*, **49**, 2379-2393. https://doi.org/10.1016/j.jacc.2007.02.059

61. House, S.D. and Lipowsky, H.H. (1988) *In Vivo* Determination of the Force of Leukocyte-Endothelium Adhesion in the Mesenteric Microvasculature of the Cat. *Circulation Research*, **63**, 658-668. https://doi.org/10.1161/01.res.63.3.658

62. Smith, M.L., Smith, M.J., Lawrence, M.B. and Ley, K. (2002) Viscosity-independent Velocity of Neutrophils Rolling on P-Selectin *in Vitro* or *in Vivo*. *Microcirculation*, **9**, 523-536. https://doi.org/10.1038/sj.mn.7800165

ABBREVIATIONS

γ_W	wall shear rate
WBCs	white blood cells
RBC	red blood cell
V_{rbc}	centerline velocity
V_{avg}	average blood flow velocity
γ	wall shear rate
V_{crit}	critical velocity
SALT	semi-automated leukocyte tracking
V_{min}	minimal velocity
V_{min}	maximal velocity
ROI	region of interest
OD	optical density
LoG	Laplacian-of-a-Gaussian
LAP	linear motion assignment problem
RMSE	root mean square error
min.	minute
sec.	seconds
Δx	displacement